Clay Minerals (2021), **56**, 87–98
doi:10.1180/clm.2021.22

CAMBRIDGE UNIVERSITY PRESS

Article

Preparation and characterization of quaternary ammonium salt and 3-aminopropyltriethoxysilane-modified sericite mica

Chunguang Xiao, Feng Lang, Yu Xiang, Yi Lin and Duxin Li*
State Key Laboratory of Powder Metallurgy, Central South University, Chang sha 410083, P.R. China

Abstract

Modified sericite mica was prepared by combining the intercalation of cetyltrimethylammonium bromide (CTAB) through ion exchange and surface modification of 3-aminopropyltriethoxysilane (KH550) with the following steps: high-temperature activation of sericite mica, acid activation, sodium modification, $LiNO_3$ treatment, the ion-exchange intercalation of the cetyltrimethylammonium cation (CTA^+) and surface modification of KH550. High-temperature activation was the most critical step for the modified sericite mica, and the number of hydroxyl groups of mica under high temperature directly affected the surface modification of KH550. The effects of various activation temperatures on the surface modification of sericite mica were investigated. The structure of activated sericite mica was intact when activation temperature was 600°C or 700°C, and the surface modification of sericite mica was not affected. The structure of activated sericite mica was partially destroyed at 800°C. The optimal temperature for activating sericite mica was 700°C. The structure and morphology of modified sericite mica were characterized by Fourier-transform infrared spectroscopy, X-ray diffraction, X-ray photoelectron spectroscopy, scanning electron microscopy, Brunauer–Emmett–Teller (BET) analysis and loose bulk volume. The KH550 could not only chemically graft onto the surface of sericite mica, but also enter into the interlayer through electrostatic attraction after its end amino group was protonated. The interlayer spacing of modified sericite mica increased to 3.22 nm, indicating that it might be an excellent layered silicate for preparing clay–polymer nanocomposites.

Keywords: activation temperature, interlayer spacing, quaternary ammonium salt, sericite mica, silane coupling agent, surface modification

(Received 31 August 2020; revised 17 June 2021; Accepted Manuscript online: 2 July 2021; Associate Editor: Margarita Darder)

Sericite mica, a layered aluminium potassium silicate ($KAl_2[AlSi_3O_{10}](OH)_2$), is a widespread clay mineral (Zhang *et al.*, 2005) composed of two Si tetrahedral sheets with a central Al octahedral sheet. Sericite mica has excellent heat resistance, electrical insulation and chemical resistance properties (Shih & Shen, 2009; Nie *et al.*, 2013), and its special nanolayer structure can not only prevent the infiltration, diffusion and transmission of the air, moisture and corrosive media, but may also play a protective role in polymer composites (Arias *et al.*, 2019; Xiao *et al.*, 2021). Therefore, sericite mica as an important functional filler had been used widely in polymer composites such as polyimide (Zhang *et al.*, 2016), polyamide (Uno *et al.*, 2009), poly(arylether ketone) (Gan *et al.*, 2001) and epoxy (Tamura *et al.*, 2008). However, sericite mica displays a poor dispersion capacity in polymer matrices due to its ease of agglomeration and poor compatibility with the polymer matrix resulting from its surface hydrophilicity, which greatly limits its application in polymers. Therefore, it was necessary to modify sericite mica to increase its dispersion in polymer matrices and its compatibility with polymers so as to improve its performance and use value (Hokkaido, 1994; Uno *et al.*, 2009).

At present, the modification of sericite mica mainly involves surface graft modification by a coupling agent and intercalation modification by an organic ammonium cation (Yang *et al.*, 1999; Gao *et al.*, 2007; Yu, 2007; Jia *et al.*, 2013; Liang *et al.*, 2013; Ding *et al.*, 2014). In addition, sericite mica particles have been covered with TiO_2 inorganic particles (Yun *et al.*, 2002; Ren *et al.*, 2007) and caesium oxide doped with synthetic calcium/mica compound silica (El-Toni *et al.*, 2006), as well as using the multi-channel encapsulation method and so on (Skale *et al.*, 2008). The modification with coupling agents improved some of the polymer's thermal and mechanical properties, but these properties were still not ideal because the compatibility between the inorganic particles of sericite mica and the polymers remained poor (Bose *et al.*, 2006; Yang *et al.*, 2008). In addition, although the modification of sericite mica with the intercalation of an organic ammonium cation facilitated its dispersion in the polymer matrix for low clay loadings and greatly improved the thermal and mechanical properties of the polymer composites (Chang *et al.*, 2007; Li *et al.*, 2011; Zhang *et al.*, 2015; Fu *et al.*, 2019; Zhao *et al.*, 2019), the problem of poor dispersion remained at greater contents of sericite mica. Therefore, in order to prepare more efficient polymer composites, it was necessary to modify sericite mica through the combination of intercalation and surface modification. In a typical intercalation process, the sericite mica is first activated at high temperatures. Subsequently, a modified sericite mica with enlarged interlayer spacing is obtained by reaction with nitric acid and a series of interlayer cation-exchange reactions that do not affect the surface modification of sericite mica (Li *et al.*, 2011; Zhang *et al.*, 2016). The hydroxyl groups of the mica react with a variety of coupling agents (Bose &

*E-mail: liduxin6404@csu.edu.cn
Cite this article: Xiao C, Lang F, Xiang Y, Lin Y, Li D (2021). Preparation and characterization of quaternary ammonium salt and 3-aminopropyltriethoxysilane-modified sericite mica. *Clay Minerals* **56**, 87–98. https://doi.org/10.1180/clm.2021.22

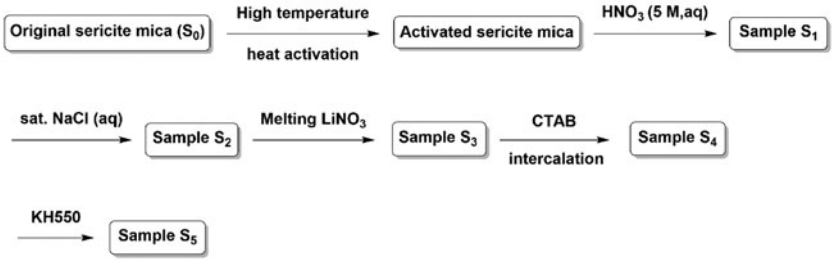

Scheme 1. Flow diagram for the preparation of CTAB and KH550-modified sericite mica.

Mahanwar, 2010; Ismail *et al.*, 2012; Ismail *et al.*, 2014). Activation through heating at high temperatures is the critical step before sericite mica can be modified by an organic ammonium cation through interlayer cation exchange. High-temperature activation affects the number of hydroxyl groups of sericite mica and directly controls the surface grafting modification. Therefore, the main targets of this study were an investigation of the effects of various activation temperatures on the sericite surface and a determination of the optimal activation temperature. Finally, cetyltrimethylammonium bromide (CTAB) and 3-aminopropyltriethoxysilane (KH550)-modified sericite mica were successfully prepared and characterized, thus contributing to an improvement of the thermal and mechanical properties of the polymer composites. A flow diagram for the preparation of CTAB and KH550-modified sericite mica is shown as Scheme 1.

Experimental

Materials

Original sericite mica (2500 mesh, Chenxing Industry Co., Ltd, Shijiazhuang, China) was washed with deionized water to remove impurities and dried for 24 h in vacuum at 100°C. The KH550 was procured from Sinopharm Chemical Reagent Co., Ltd (China) and the CTAB was supplied by the China National Medicine Group. Other reagents were commercially available and used without further purification.

High-temperature activation and surface grafting modification of sericite mica

In order to investigate the effect of activation temperature on the surface modification of sericite mica so as to determine the optimal activation temperature, the following experiments were carried out:

(1) The original sericite mica (S_0) was thermally activated at 600°C, 700°C and 800°C for 1 h and then cooled to room temperature. The activated sericite mica powders obtained were named S_{600}, S_{700} and S_{800}, respectively.
(2) A certain amount of original sericite mica and the above activated sericite mica powder were placed into a three-necked flask and deionized water (15 mL) and ethanol (15 mL) were added. Then, the sericite mica was dispersed evenly by magnetic stirring, and the pH was adjusted to ~3–4 by adding acetic acid. Subsequently, KH550 (10 wt.% of the activated sericite mica powder) was added dropwise at room temperature. The mixture was stirred continually for 12 h and then was heated to 70°C for 3 h and cooled to room temperature. The reaction mixture was filtered and the filter cake was washed with deionized water and ethanol three times and dried in vacuum at 60°C for 5 h. The surface-modified sericite mica powders obtained were labelled KH550-S_0, KH550-S_{600}, KH550-S_{700} and KH550-S_{800}.

Preparation of CTAB and KH550-modified sericite mica

The CTAB and KH550-modified sericite mica were prepared from the activated sericite mica obtained at the optimal temperature described above according to the multistep reaction (Scheme 1) as follows:

(1) The activated sericite mica (25 g) obtained under the optimal temperature was leached with 5 M HNO_3 solution under stirring for 5 h at 95°C and cooled to room temperature. The reaction solution was filtered and the filter cake was washed with deionized water several times and dried in vacuum at 80°C for 12 h. The resulting acidified sericite mica sample was labelled S_1.
(2) The sample S_1 (20 g) was reacted with saturated NaCl solution under stirring for 12 h at 120°C and cooled to room temperature. The solution was filtered and the filter cake was washed with deionized water several times and dried in vacuum at 80°C for 12 h. The resulting sericite mica sample was labelled S_2.
(3) A mixture of sample S_2 (10 g) and $LiNO_3$ powder (200 g) was mixed thoroughly for 0.5 h then heated to 350°C in a furnace for 48 h and cooled to room temperature. Then, the mixture was added to deionized water (800 mL) and filtered, and the filter cake was washed with deionized water several times and dried in vacuum at 80°C for 12 h. The resulting sericite mica sample had a cation-exchange capacity of 60 $cmol^+ kg^{-1}$ and was labelled S_3.
(4) A total of 5 g of S_3 was dispersed evenly in 600 mL of deionized water, then the intercalating agent CTAB (16.4 g, 45.0 mmol) was added. The mixture was heated at 150°C for 3 days under vigorous stirring, cooled to room temperature and filtered. The filter cake was washed repeatedly with deionized water to remove excess CTAB, and the filter cake was dried in vacuum at 80°C for 12 h. The sericite mica sample obtained was labelled S_4.
(5) A total of 3 g of sample S_4 was dispersed in deionized water (15 mL) and ethanol (15 mL). The pH was adjusted to ~3–4 with acetic acid, and KH550 (0.3 g) was added dropwise at room temperature. The mixture remained under stirring for 12 h, then heated at 70°C for 3 h, cooled to room temperature and filtered. The filter cake was washed repeatedly with deionized water and dried in vacuum at 60°C for 5 h. The modified sericite mica sample obtained was labelled S_5.

Characterization

Fourier-transform infrared (FTIR) spectra were recorded on a Nicolet MAGNA-IR 750 spectrometer using KBr discs or thin

https://doi.org/10.1180/clm.2021.22 Published online by Cambridge University Press

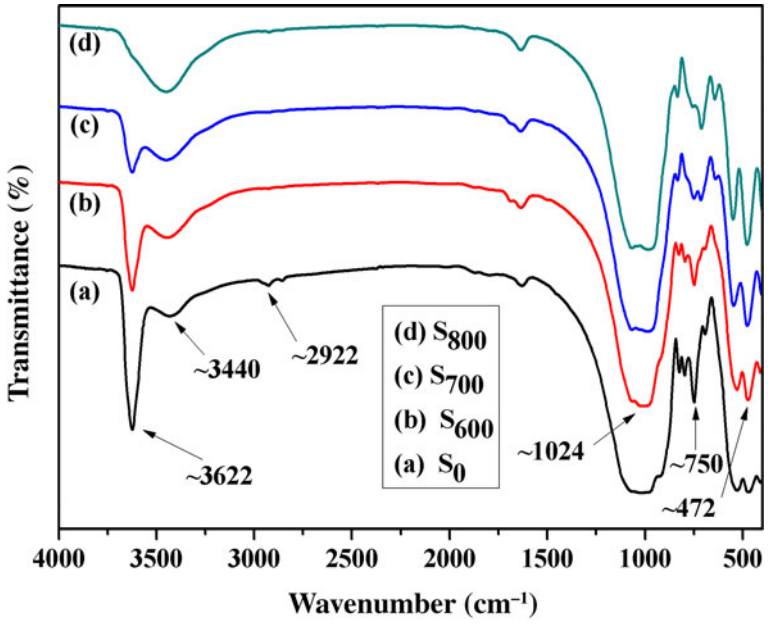

Fig. 1. FTIR spectra of (a) S_0, (b) S_{600}, (c) S_{700} and (d) S_{800}.

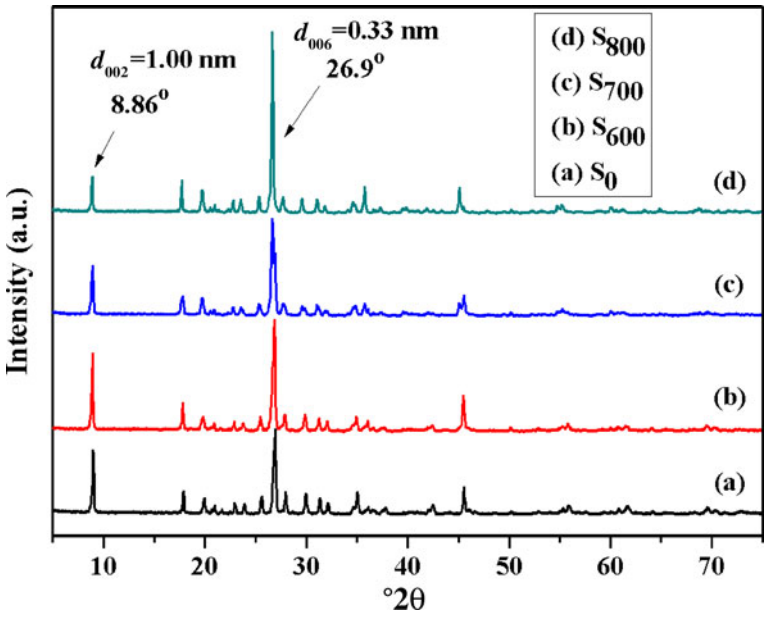

Fig. 2. XRD traces of (a) S_0, (b) S_{600}, (c) S_{700} and (d) S_{800}.

films. An X-ray diffraction (XRD) study was performed on a Rigaku D/Max 2550 instrument at 40 kV and 250 mA with Cu-*K*α radiation. The experiments were performed in the range of ~5–75°2θ with a step size of 0.02° at a scanning rate of 3° min^{-1}. A scanning electron microscopy (SEM) study was performed with an FEI Quanta FEG 250 instrument on gold-coated samples. X-ray photoelectron spectroscopy (XPS) analysis was performed using a K-Alpha 1063 spectrometer with an Al-K X-ray source to determine the accurate binding energies of elements. Thermogravimetric analysis (TGA) curves were obtained on a NETZSCH STA 449C thermal analyser on samples heated in an alumina crucible at a rate of 10°C min^{-1} from 50 to 900°C in an argon atmosphere. The specific surface area of the modified sericite mica was determined by N_2 adsorption–desorption isotherms at –196°C with a multistation specific surface area and porosity analyser (Model ASAP 2460; Micromeritics, USA). The samples were degassed at 70°C for 12 h prior to analysis.

Results and discussion

The effects of various activation temperatures on the surface modification of sericite mica

FTIR spectra of the original and activated sericite mica

Figure 1 shows the FTIR spectra of the original and activated sericite mica. The absorption bands at ~472 and 800 cm^{-1} are assigned to Al–O and Si–O stretching and bending, respectively. The band near 1024 cm^{-1} is assigned to Si–O–Si stretching (Zhang *et al.*, 2016). The two absorption bands at ~3445 and 3622 cm^{-1} were assigned to the –OH stretching vibration of

https://doi.org/10.1180/clm.2021.22 Published online by Cambridge University Press

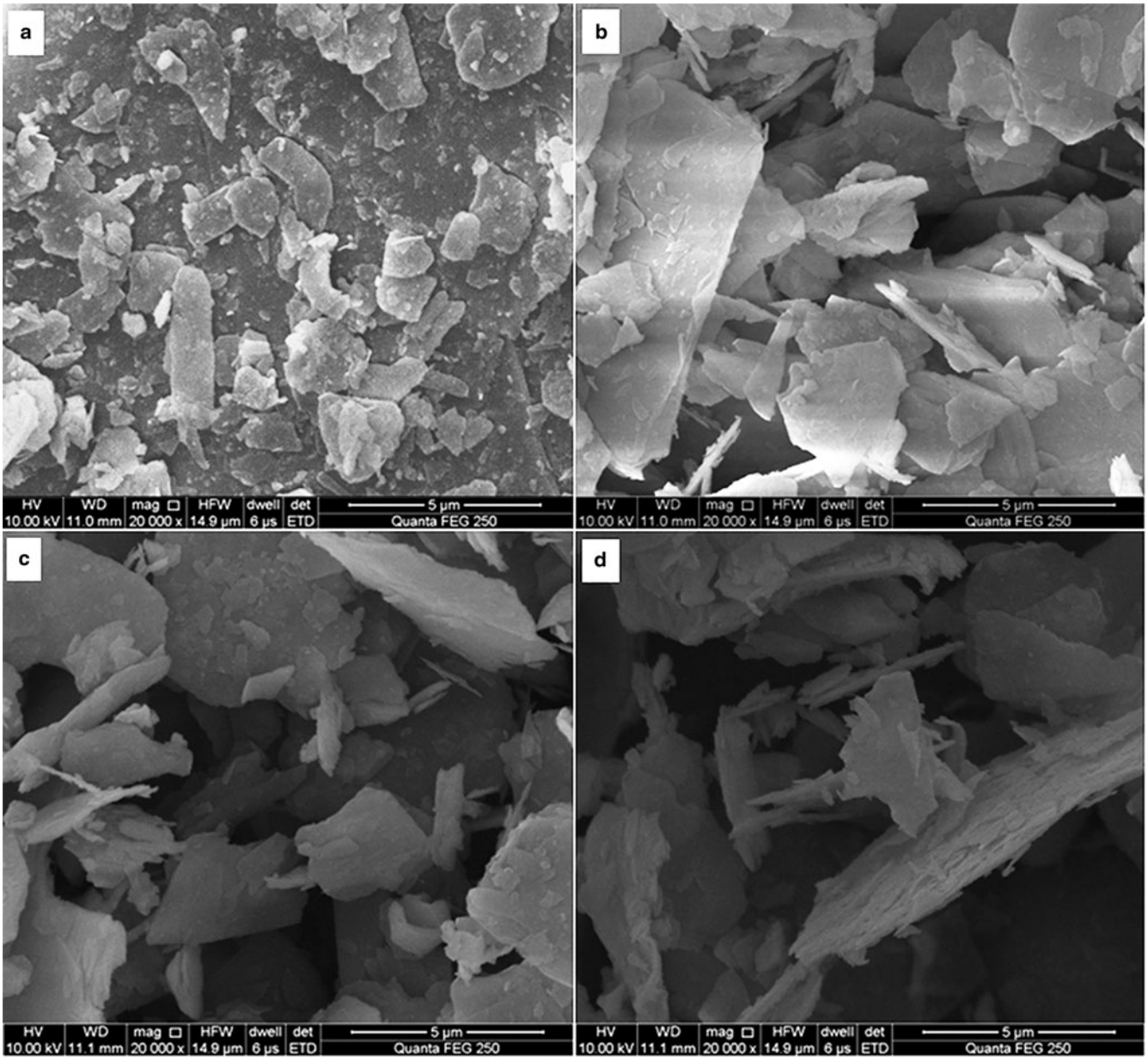

Fig. 3. SEM images of (a) S_0, (b) S_{600}, (c) S_{700} and (d) S_{800}.

adsorbed water and the stretching of the lattice OH of sericite mica, respectively. After the original mica was activated at 600°C, 700°C and 800°C, the structure did not seem to be affected, but the intensity of the absorption band near 3622 cm^{-1} decreased gradually with the increase in the activation temperature due to dehydroxylation. The band at ~3622 cm^{-1} of S_{800} almost disappeared, indicating almost total dehydroxylation. However, the absorption band at 3440 cm^{-1} did not disappear, indicating that there was still adsorbed water present.

XRD of the original and activated sericite mica

The XRD traces of S_0, S_{600}, S_{700} and S_{800} are shown in Fig. 2. Two major sharp basal diffraction peaks at 8.86 and 26.9°2θ (corresponding to *d* spacings of 1.00 and 0.33 nm, respectively) dominate the XRD traces of S_{600}, S_{700} and S_{800}. The XRD traces of S_{600} and S_{700} are comparable to those of S_0. However, the intensity of the 001 diffraction peak at 8.86°2θ decreased significantly compared to those of S_0, S_{600} and S_{700}, while the intensity of the diffraction peak at 26.9°2θ increased significantly. The XRD results suggest that the temperature of 800°C might be too high for the activation of sericite mica.

SEM study of the original and activated sericite mica

Figure 3 shows SEM images of the original and activated sericite mica. The particles of S_0 are tightly stacked and the crystal surface is flat with a smooth morphology. After activation at 600°C, the sericite particles (S_{600}) became looser, stacking was destroyed and the particle edges were blurred. After heating at 700°C, the S_{700} particles became more disordered and their edges displayed cracks. After heating at 800°C, the surface of S_{800} particles became more blurred and the particle edges grew curved, which indicated partial structural disruption, in accord with the XRD results.

https://doi.org/10.1180/clm.2021.22 Published online by Cambridge University Press

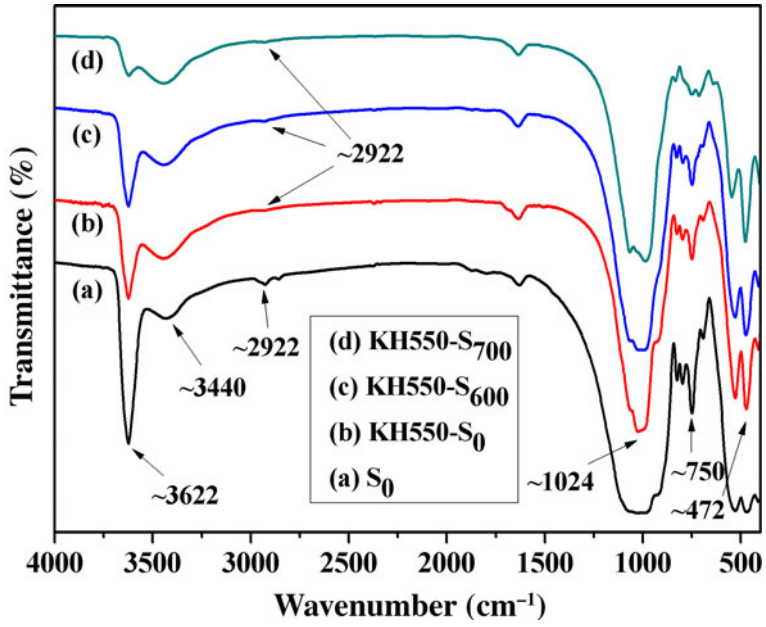

Fig. 4. FTIR spectra of (a) S_0, (b) KH550-S_0, (c) KH550-S_{600} and (d) KH550-S_{700}.

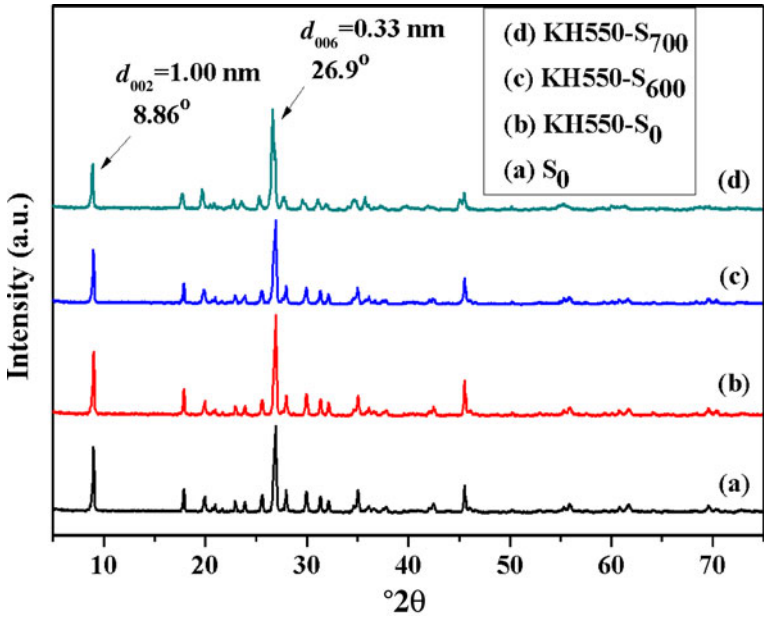

Fig. 5. XRD traces of (a) S_0, (b) KH550-S_0, (c) KH550-S_{600} and (d) KH550-S_{700}.

The aforementioned results suggest that the activation temperature for sericite mica should not exceed 700°C. In order to select the optimal thermal activation temperature, the effects of KH550 on the surface modification of S_{600} and S_{700} were further investigated.

FTIR spectra of S_0, KH550-S_0, KH550-S_{600} and KH550-S_{700}

The FTIR spectra of S_0, KH550-S_0, KH550-S_{600} and KH550-S_{700} are shown in Fig. 4. Comparing Figs 1 and 4, modification of the activated sericite mica with KH550 reduced significantly the intensity of the band at 3622 cm^{-1}, whereas the band at 1024 cm^{-1} became sharper compared to S_0, suggesting that KH550 reacted with the –OH of sericite mica and that KH550 was grafted successfully onto the sericite surface. The intensity of the –OH stretching band at 3622 cm^{-1} in samples KH550-S_{600} and KH550-S_{700} decreased compared to that of KH550-S_0, probably due to the greater surface grafting rate of KH550 on S_{600} and S_{700} compared to S_0. The grafting rate of KH550-S_{700} was greater due to the increased dehydroxylation caused by the greater activation temperature, and it was possible to reduce the grafting rate of KH550 on the sericite mica surface. In addition, previous work has shown that the specific surface area of the sericite mica increases after activation at high temperature, and the greater the activation temperature, the greater the specific surface area (Lalhmunsiama *et al.*, 2015), which is in accordance with the present work. Furthermore, the FTIR spectra of S_0, KH550-S_0, KH550-S_{600} and KH550-S_{700} showed few differences (Fig. 4).

After modification of activated sericite mica by KH550, a new weak band appeared at ~2922 cm^{-1}, assigned to –CH_2– from

https://doi.org/10.1180/clm.2021.22 Published online by Cambridge University Press

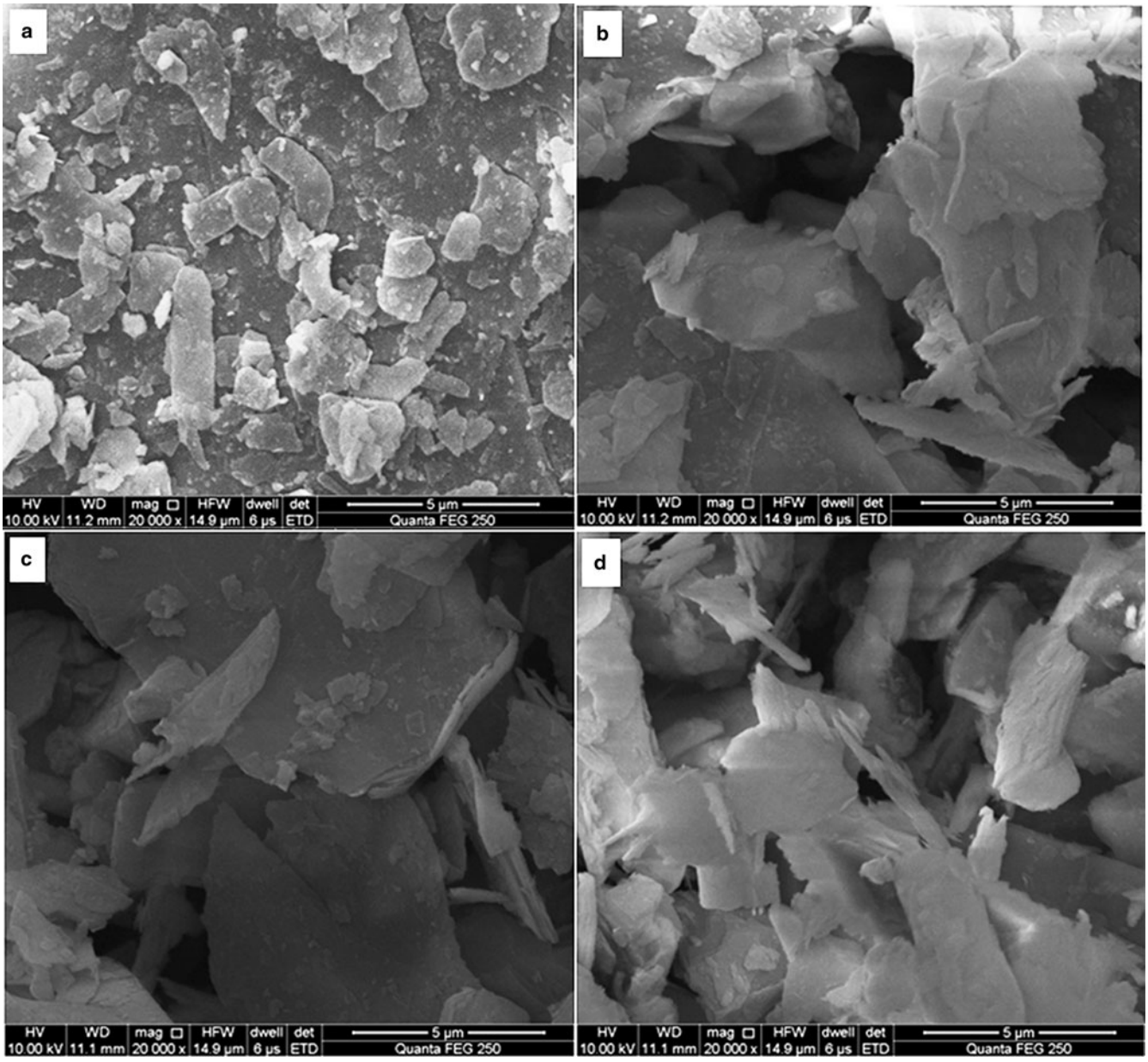

Fig. 6. SEM images of (a) S_0, (b) KH550-S_0, (c) KH550-S_{600} and (d) KH550-S_{700}.

KH550. The FTIR spectrum of S_0 also contained a weak absorption band near 2922 cm^{-1}, assigned to organic agents added during the beneficiation process. The spectra of high-temperature-activated sericite mica did not contain the absorption band at ~2922 cm^{-1} (Fig. 1), indicating that KH550 was successfully grafted onto the sericite mica surface. In addition, the spectra of sericite modified by KH550 did not display a C–N absorption band (Fig. 4) due to the low additive amount of KH550 and the weak absorption band of $–NH_2$.

After modification of S_0, S_{600} and S_{700} by KH550, the absorption bands of sericite mica at 472, 750 and 1024 cm^{-1} were not affected, suggesting that the structure of sericite mica was not affected (Fig. 4). Similarly, the intensity of the absorption band of adsorbed water at 3440 cm^{-1} was not affected, indicating that the surface modification of sericite mica with KH550 did not affect water adsorption. In brief, KH550 was grafted onto the surface of sericite mica by chemical bonding and did not affect the structure of sericite mica.

XRD study of S_0, KH550-S_0, KH550-S_{600} and KH550-S_{700}

The XRD traces of S_0, KH550-S_0, KH550-S_{600} and KH550-S_{700} are shown in Fig. 5. The diffraction maxima of KH550-S_0, KH550-S_{600} and KH550-S_{700} did not change significantly after modification with KH550 (cf. Figs 2 & 5). Therefore, the surface of S_0 could still be chemically modified with KH550 after high-temperature activation. In addition, after modification of the original and activated sericite mica by KH550, the structure of sericite mica did not change, but the KH550 was grafted onto the surface of sericite mica. However, the optimal activation temperature was not identified using XRD analysis.

https://doi.org/10.1180/clm.2021.22 Published online by Cambridge University Press

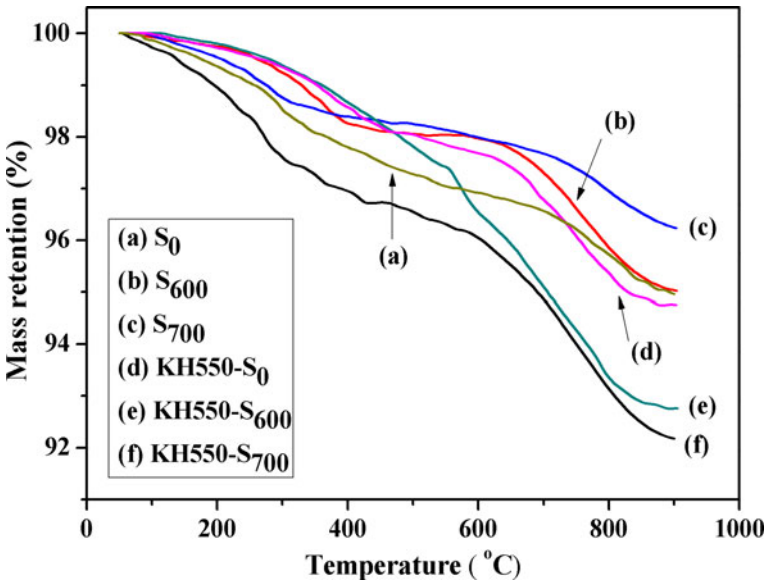

Fig. 7. TGA curves of (a) S_0, (b) S_{600}, (c) S_{700}, (d) KH550-S_0, (e) KH550-S_{600} and (f) KH550-S_{700}.

SEM images of S_0, KH550-S_0, KH550-S_{600} and KH550-S_{700}

The surface morphology of the sericite mica powder was used as a proxy for determining the optimum activation temperature. The SEM images of S_0, KH550-S_0, KH550-S_{600} and KH550-S_{700} are shown in Fig. 6. After the original or activated sericite mica was modified by KH550, its surface became blurred (Fig. 6). The surface of KH550-S_{700} became more blurry, and its grain-stacking state was looser than that of KH550-S_{600}, indicating that 700°C was the optimal activation temperature.

TGA analysis of S_0, S_{600}, S_{700}, KH550-S_0, KH550-S_{600} and KH550-S_{700}

Figure 7 shows the TGA curves of S_0, S_{600}, S_{700}, KH550-S_0, KH550-S_{600} and KH550-S_{700}. S_0, S_{600} and S_{700} display a mass loss event at <200°C due to evaporation of the adsorbed water, a second mass loss at ~200–600°C due to the removal of tightly bound water and a third mass loss at ~600–900°C due to dehydroxylation (Heller-Kallai, 2006; Samakande *et al.*, 2007). The second event is more pronounced in S_0. Thermal degradation of KH550 grafted onto the surface of sericite mica also occurred at ~200–600°C; hence, the mass loss of KH550-S_0 at ~200–600°C is due to the decomposition of KH550 and release of tightly bound water. The mass loss rate of KH550-S_0 at ~200–600°C was lower than that of S_0, probably because the KH550 was tightly bound on the surface of the sericite layers and so physically blocked the release of the adsorbed water. In addition, KH550-S_{700} displayed a greater thermal mass loss rate than those of KH550-S_{600} and KH550-S_0 (Fig. 7), probably due to the greater specific surface area and grafting rate of KH550 compared to those of KH550-S_{600} and KH550-S_0 (Lalhmunsiama *et al.*, 2015). Hence, the optimal activation temperature for sericite mica was 700°C.

Characterization of CTAB and KH550-modified sericite mica

FTIR spectra of S_0, S_4 and S_5

The original sericite mica was activated at 700°C and subsequently modified with CTAB and KH550 through multistep reaction conditions. Figure 8 shows the FTIR spectra of S_0, S_4 and S_5. After modification with CTAB, new bands appeared at 2922 and 2852 cm^{-1}, assigned to $-CH_2-$ and $-CH_3$, respectively, and at 1414 and 1474 cm^{-1}, assigned to quaternary ammonium salt, indicating that CTA^+ was successfully intercalated into the sericite mica. The FTIR spectrum of S_5 was similar to that of S_4 because the characteristic bands of the organic groups of KH550 grafted onto the surface of sericite mica were similar to those of CTA^+.

XRD study of S_0, S_3, S_4 and S_5

The XRD traces of S_0, S_3, S_4 and S_5 are shown in Fig. 9. After the activated sericite mica S_{700} was treated with $LiNO_3$, the d_{002} of S_3 increased to 1.22 nm, which was beneficial for the intercalated reaction of the organic ammonium cation in the next step (Yu *et al.*, 2006). After S_3 was treated with CTAB, the d_{002} of the S_4 obtained increased further to 2.78 nm. Finally, after treatment of S_4 with KH550, the d_{002} increased to 3.22 nm, suggesting that KH550 not only modified the surface of the sericite mica, but was also intercalated in the interlayer. This is because the terminal amino group of KH550 was protonized under acidic conditions, entering the interlayer of sericite mica through ion exchange (Lai *et al.*, 2014). The observed *d*-spacings were greater than those reported in previous work under the same modification conditions or using other intercalation agents (Theng, 2012; Ding *et al.*, 2014; Zawrah *et al.*, 2014; Zhang *et al.*, 2015; Siregar *et al.*, 2018). In addition, there is limited previous work on the comprehensive treatment of sericite mica combining intercalation and surface modification.

XPS spectra of S_4 and S_5

X-ray photoelectron spectroscopy was employed to investigate the changes in N1*s* before and after modification of S_4 with KH550. The XPS spectra of S_4 and S_5 and their high-resolution spectra of the N1*s* of S_4 and S_5 are depicted in Fig. 10. In the XPS spectra of S_4 and S_5, the N atom percentages increased from 1.93% (S_4) to 2.76% (S_5), indicating successful introduction of KH550 (Fig. 10a). To understand the synthesis principle further, deconvolution of high-resolution spectra (N1*s*) was performed. After S_4 reacted with KH550, a new shoulder peak appeared in the high-resolution spectra of the N1*s* of S_5 (Fig. 10b). Three peaks appeared in the N1s of S_5 (Fig. 10c), assigned to $-NH_2$ (399.4 eV), $C-N^+$ (401.2 eV) and C–N (402.4 eV). These data

https://doi.org/10.1180/clm.2021.22 Published online by Cambridge University Press

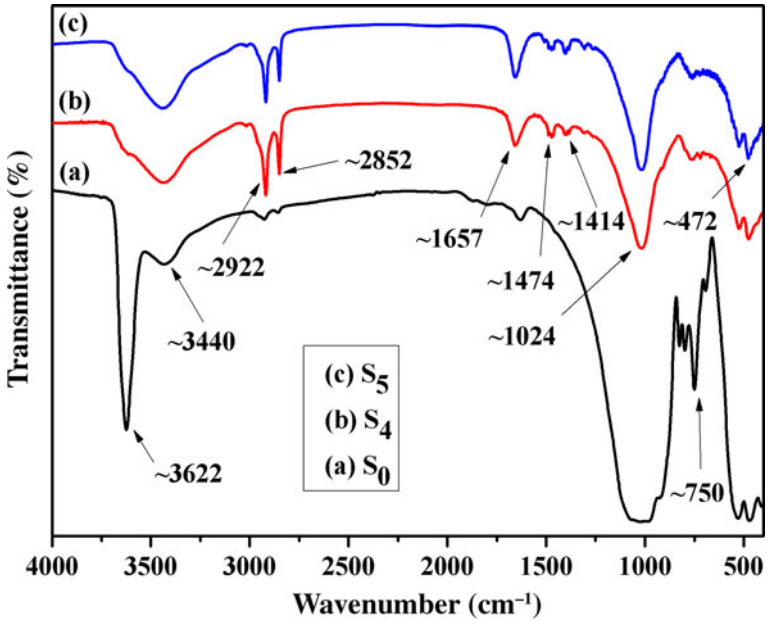

Fig. 8. FTIR spectra of (a) S_0, (b) S_4 and (c) S_5.

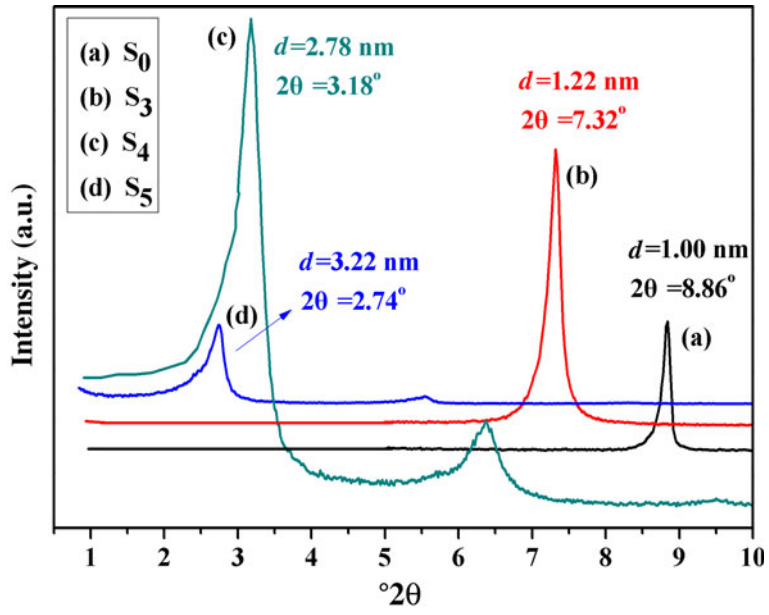

Fig. 9. XRD traces of (a) S_0, (b) S_3, (c) S_4 and (d) S_5.

indicate that KH550 successfully grafted by chemical reaction with oxygen groups on the S_4 surface, and the new shoulder peak of the N1*s* of S_5 might be attributed to the peak of $-NH_2$ from KH550.

SEM images of S_4 and S_5

The surface morphology of S_4 and S_5 was studied using SEM (Fig. 11). The mica particles in S_0 are smaller and blockier compared to those of S_4 and S_5 (Figs 6a and 11). Although the sizes of S_4 and S_5 particles were slightly greater than that of their S_0 counterpart, the particles formed thin layers, suggesting that the structure of sericite mica changed due to the exchange reaction between CTAB and the interlayer cations. The particles in S_4 were attached close to each other and have a clear surface, while the particles in S_5 were more loosely compacted than their counterparts in S_4, and the thin sheet surface and edges of the S_5 particles were more blurred, further demonstrating that KH550 had been grafted successfully onto the surface of S_4 (Fig. 11).

Brunauer–Emmett–Teller analysis of S_0, S_4 and S_5

The nitrogen adsorption isotherms of S_0, S_4 and S_5 are shown in Fig. 12. The isotherms are type IV with a H3 hysteresis loop, suggesting the presence of mesopores (Lalhmunsiama *et al.*, 2015). The nitrogen adsorption–desorption isotherm of S_0 showed the smallest hysteresis loop, whereas the isotherm of S_5 showed the largest hysteresis loop, suggesting an increase in mesoporosity of sericite (Pawar *et al.*, 2013). The specific surface area of sericite increased significantly after modification of CTAB and KH550, and the Brunauer–Emmett–Teller (BET) specific surface areas

https://doi.org/10.1180/clm.2021.22 Published online by Cambridge University Press

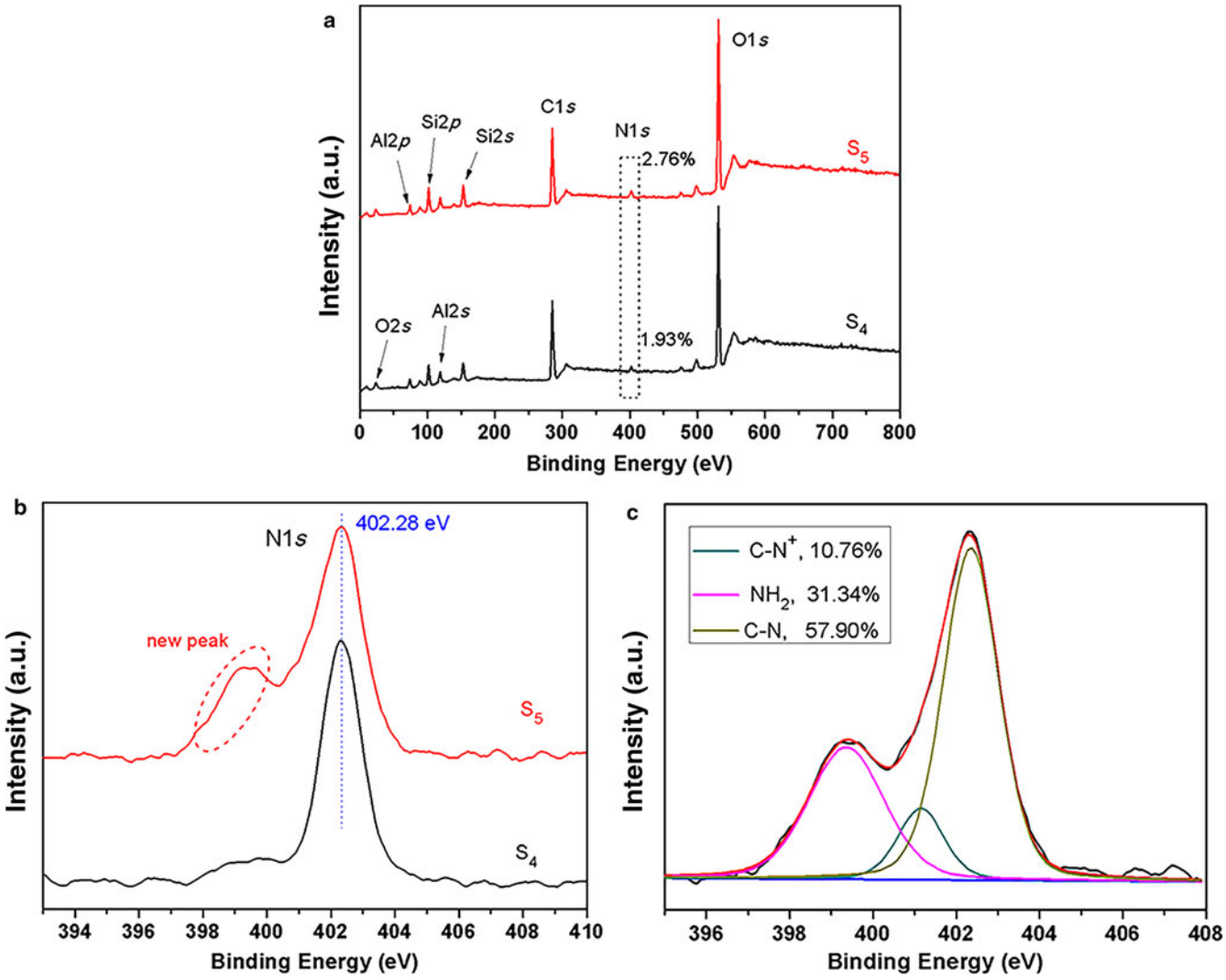

Fig. 10. (a) XPS survey spectra of S_4 and S_5 and high-resolution spectra of the N1*s* of (b) S_4 and S_5 and (c) S_5.

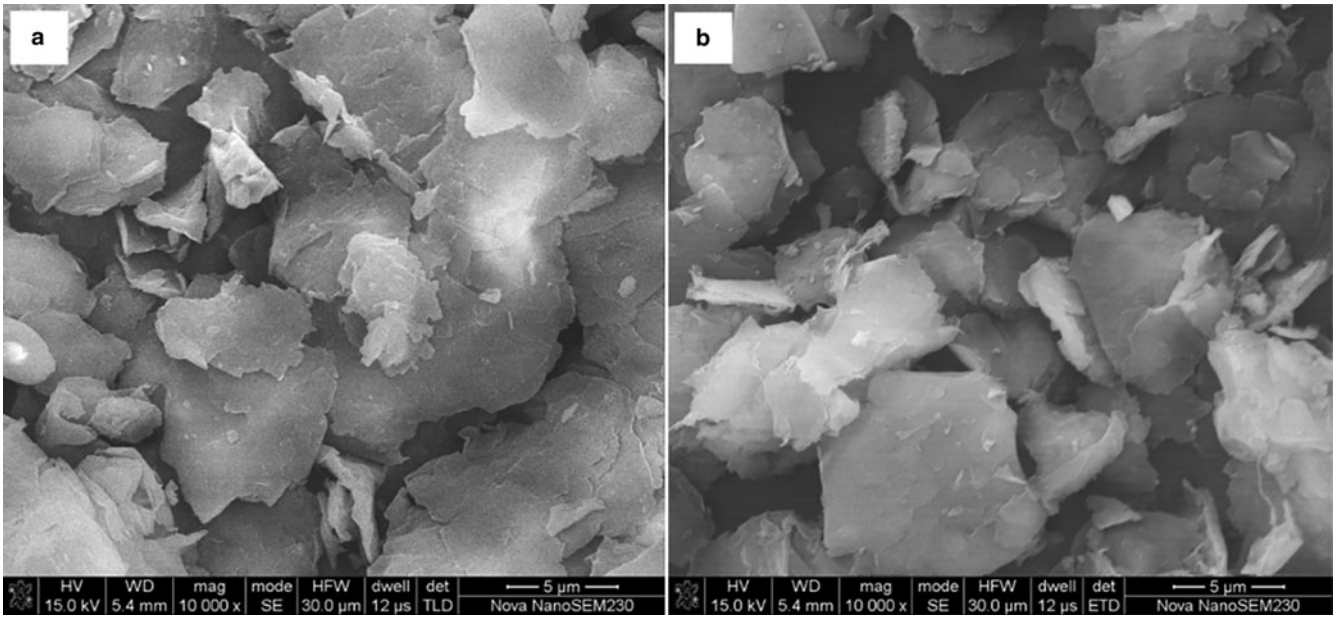

Fig. 11. SEM images of (a) S_4 and (b) S_5.

https://doi.org/10.1180/clm.2021.22 Published online by Cambridge University Press

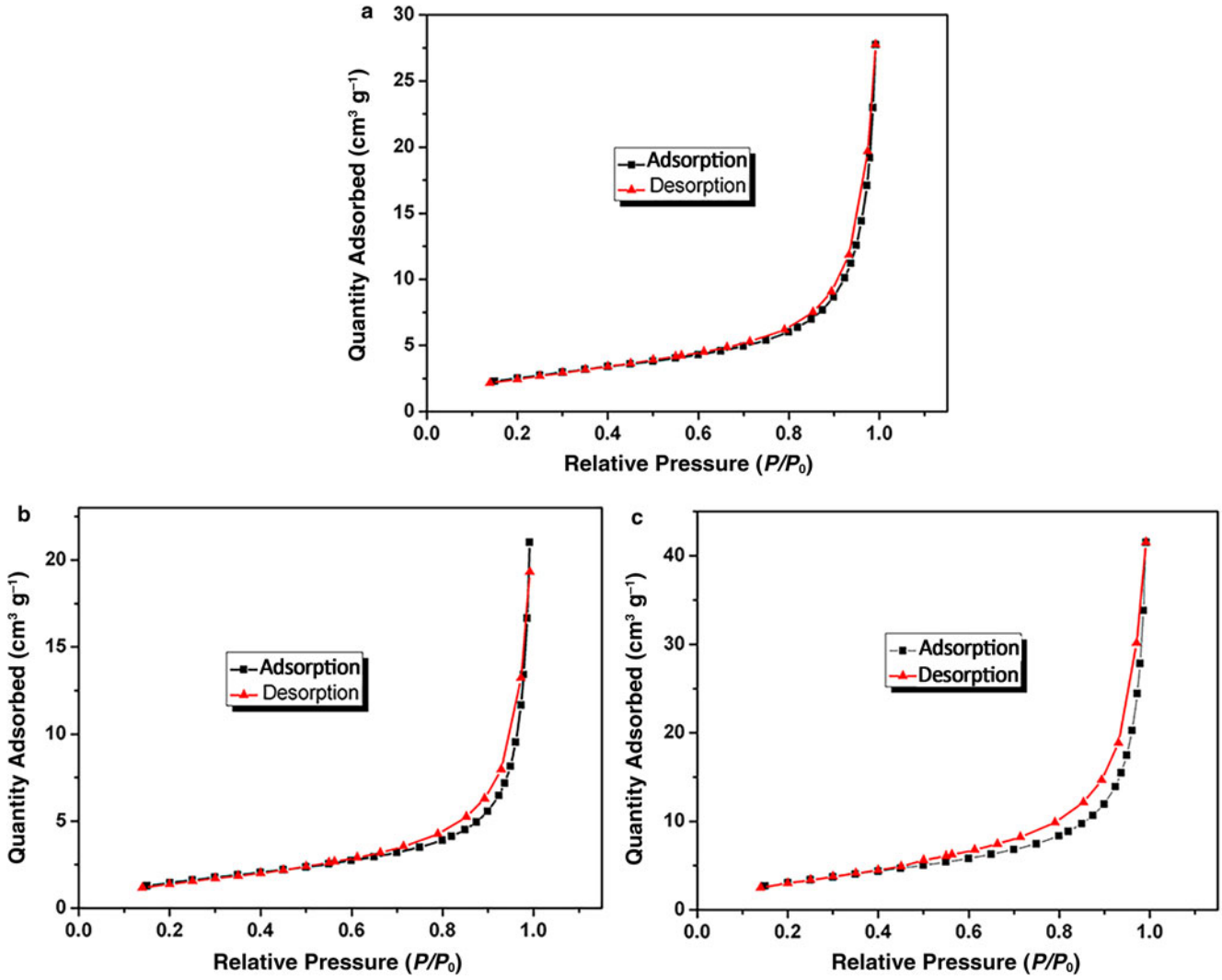

Fig. 12. Nitrogen adsorption isotherms of (a) S_0, (b) S_4 and (c) S_5.

of S_0, S_4 and S_5 were 9, 5 and 12 $m^2\ g^{-1}$, respectively. In addition, the pore sizes of S_0, S_4 and S_5 were 2.23, 2.03 and 3.60 nm, respectively, corresponding to pore volumes of 0.043, 0.032, and 0.064 $cm^3\ g^{-1}$, respectively. S_0 had a greater BET specific surface area and pore volume than S_4 because the intercalation of organic ammonium ions caused aggregation of sericite particles. In contrast, the introduction of KH550 disaggregated sericite particles, so S_5 had the greatest BET specific surface area and pore volume. At the same time, some KH550 molecules entered the layers of sericite, further increasing the pore size and specific surface area, contributing to greater dispersion of S_5 particles.

The loose powder state of S_0, S_4 and S_5

The loose bulk volumes of 1 g of S_0 and S_4 were 2.50 and 1.70 mL, corresponding to loose bulk densities of 0.40 and 0.59 g mL^{-1}, respectively (Fig. 13 & Table 1). This suggests that the loose bulk volume and pores between the particles in S_4 were smaller and that the aggregate of the sheet layers was more compact than in S_0 (Fig. 11a). This is attributed to the fact that organic ammonium cations entered the interlayer of sericite and enlarged its interlayer spacing, causing aggregation of sericite particles. In addition, the loose bulk volume of 1 g of S_5 was greater and the loose bulk density was smaller than those of S_0 and S_4, indicating that the structure of S_5 was very loose and easy to disperse (Fig. 11b). This might be because chain hydrocarbons on the surface of sericite mica prevented sheet layers from accumulating with each other after modification of S_4 by KH550. However, there is limited previous work on the loose state of sericite mica.

Conclusions

Sericite mica was modified by combining the intercalation of CTAB through ion exchange and surface modification with KH550. The effects of various activation temperatures on the surface modification of sericite were investigated. The number of hydroxyls of sericite decreased with increasing activation temperature, but the structure was almost unaffected when thermal activation was conducted at <600°C and 700°C. In contrast, the structure of sericite was partially destroyed at 800°C. After the activated sericite mica was modified by KH550, the decrease in the number of hydroxyls did not affect the grafting of KH550. S_{700} displayed a greater grafting rate of KH550 than S_{600} and S_0. The optimal activation temperature of sericite was 700°C. KH550 was not only chemically grafted onto the surface of

https://doi.org/10.1180/clm.2021.22 Published online by Cambridge University Press

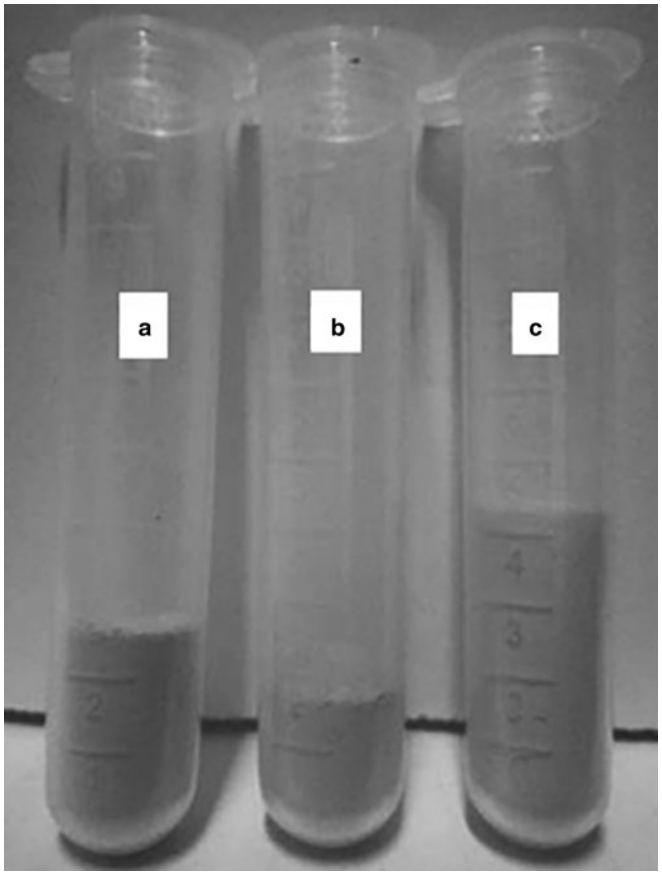

Fig. 13. Swelling volumes of 1 g of (a) S_0, (b) S_4 and (c) S_5.

Table 1. The loose bulk volume and density data for S_0, S_4 and S_5.

Sample	Weight (g)	Loose bulk volume (mL)	Loose bulk density (g mL^{-1})
S_0	1.0	2.50	0.40
S_4	1.0	1.70	0.59
S_5	1.0	4.30	0.23

sericite particles, but also entered the sericite mica interlayer through electrostatic attraction after the end amino groups were protonated. The interlayer spacing of modified sericite mica increased to 3.22 nm, yielding a greater loose bulk volume. The preparation of modified sericite mica would be of great value for improving its dispersion in polymer matrices and its compatibility with polymers, as well as for developing clay–polymer nanocomposites for various applications.

Financial support. This work was supported financially by the Key Research and Development Project of Hunan Province 'Research on Key Technologies of Advanced Functional Polyimide Materials' under Grant Number 2018GK2063.

References

Arias J.J.R., Rosa J. & Marques M.F.V. (2019) Influence of phyllosilicate structure on performance of polypropylene nanocomposites prepared *via in-situ* polymerization. *Journal of Nanoscience and Nanotechnology*, **19**, 1908–1922.

Bose S. & Mahanwar P.A. (2010) Effects of titanate coupling agent on the properties of mica-reinforced nylon-6 composites. *Polymer Engineering & Science*, **45**, 1479–1486.

Bose S., Raghu H. & Mahanwar P.A. (2006) Mica reinforced nylon-6: effect of coupling agents on mechanical, thermal, and dielectric properties. *Journal of Applied Polymer Science*, **100**, 4074–4081.

Chang J.H., Mun M.K. & Kim J.C. (2007) Synthesis and characterization of poly(butylene terephthalate)/mica nanocomposite fibers *via in situ* interlayer polymerization. *Journal of Applied Polymer Science*, **106**, 1248–1255.

Ding H., Wang Y.B., Liang Y. & Qin F.X. (2014) Preparation and characterization of cetyl trimethylammonium intercalated sericite. *Advances in Materials Science and Engineering*, **2014**, 1–8.

El-Toni A.M., Yin S. & Sato T. (2006) Synthesis and silica coating of calcia-doped ceria/mica nanocomposite by seeded polymerization technique. *Applied Surface Science*, **252**, 5063–5070.

Fu Y.J., Wang Y.X., Wang S., Gao Z.D.F. & Xiong C. X. (2019) Enhanced breakdown strength and energy storage of PVDF-based dielectric composites by incorporating exfoliated mica nanosheets. *Polymer Composites*, **40**, 2088–2094.

Gan D., Lu S., Song C. & Wang Z. (2001) Mechanical properties and frictional behavior of a mica-filled poly(aryl ether ketone) composite. *European Polymer Journal*, **37**, 1359–1365.

Gao H.M., Yuan J.Z., Wang X.R., Guan J.F., Zhang L.Y., Jing Z.Q. & Mao Y.L. (2007) Mechanism of surface modification for sericite. *Journal of Wuhan University of Technology*, **22**, 470–472.

Heller-Kallai L. (2006) Thermally modified clay minerals. *Developments in Clay Science*, **1**, 289–308.

Hokkaido J.M. (1994) *Surface Modification Power Technology Handbook*. Butterworth, London, UK, pp. 453–457.

Ismail H., Hamid Z.A.A. & Ishak S. (2012) Effect of silane coupling agent on the curing, tensile, thermal, and swelling properties of EPDM/mica composites. *Advanced Materials Research*, **626**, 641–651.

Ismail H., Ishak S. & Hamid Z.A.A. (2014) Effect of silane coupling agent on the curing, tensile, thermal, and swelling properties of ethylene–propylene–diene monomer rubber (EPDM)/mica composites. *Journal of Vinyl and Additive Technology*, **20**, 116–121.

Jia Z.M., Chen S.J. & Zhang J. (2013) Preparation and properties of polydimethylsiloxane–mica composites. *Journal of Applied Polymer Science*, **127**, 3017–3025.

Lai D.W., Li D.X., Yang J. & Yang L. (2014) Preparation and characterization of quaternary ammonium complex silane coupling agent modified montmorillonite. *Bulletin of the Chinese Ceramic Society*, **33**, 1298–1302.

Lalhmunsiama, Tiwari D. & Lee S.M. (2015) Physico-chemical studies in the removal of Sr(II) from aqueous solutions using activated sericite. *Journal of Environmental Radioactivity*, **147**, 76–84.

Li S.Y., Chen Q., Wu S.H. & Shen J. (2011) Studies of modification of HDPE and interfacial interaction of its composites with sericite. *Polymers for Advanced Technologies*, **22**, 2517–2522.

Liang Y., Ding H., Wang Y.B., Liang N. & Wang G.L. (2013) Intercalation of cetyl trimethylammonium ion into sericite in the solvent of dimethyl sulfoxide. *Applied Clay Science*, **74**, 109–114.

Nie Y.M., Wei S.B., Lu X.L. & Liu S.X. (2013) Research of sericite in mineral technology. *Advanced Materials Research*, **721**, 350–353.

Pawar R.R., Kevadiya B.D., Brahmbhatt H. & Bajaj H.C. (2013) Template free synthesis of mesoporous hectorites: efficient host for pH responsive drug delivery. *International Journal of Pharmaceutics*, **446**, 145–152.

Ren M., Yin H.B., Wang A.L., Jiang T.S. & Wada Y.J. (2007) Mica coated by direct deposition of rutile TiO_2 nanoparticles and the optical properties. *Materials Chemistry and Physics*, **103**, 230–234.

Samakande A., Hartmann P.C., Cloete V. & Sanderson R.D. (2007) Use of acrylic based surfmers for the preparation of exfoliated polystyrene–clay nanocomposites. *Polymer*, **48**, 1490–1499.

Shih Y.J. & Shen Y.H. (2009) Swelling of sericite by $LiNO_3$-hydrothermal treatment. *Applied Clay Science*, **43**, 282–288.

Siregar S.H., Wijaya K., Kunarti E.S., Syoufian A. & Suyanta S. (2018) Preparation and characterization of montmorillonite–cetyl trimethylammonium bromide. *Asian Journal of Chemistry*, **30**, 25–28.

https://doi.org/10.1180/clm.2021.22 Published online by Cambridge University Press

Skale S., Doleček V. & Slemnik M. (2008) Electrochemical impedance studies of corrosion protected surfaces covered by epoxy polyamide coating systems. *Progress in Organic Coatings*, **62**, 387–392.

Tamura K., Yokoyama S., Pascua C.S. & Yamada H. (2008) New age of polymer nanocomposites containing dispersed high-aspect-ratio silicate nanolayers. *Chemistry of Materials*, **20**, 2242–2246.

Theng B.K.G. (2012) Polymer–clay nanocomposites. *Developments in Clay Science*, **4**, 201–241.

Uno H., Tamura K., Yamada H., Umeyama K., Hatta T. & Moriyoshi Y. (2009) Preparation and mechanical properties of exfoliated mica–polyamide 6 nanocomposites using sericite mica. *Applied Clay Science*, **46**, 81–87.

Xiao C.G., Li D.X., Zeng D., Lang F., Xiang Y. & Lin Y. (2021) A comparative investigation on different silane coupling agents modified sericite mica/polyimide composites prepared by *in situ* polymerization. *Polymer Bulletin*, **78**, 863–883.

Yang R., Yu J., Liu Y. & Wang K.H. (2008) Effects of coupling agents on the natural aging behavior and oxidation profile of high-density polyethylene/sericite composites. *Journal of Applied Polymer Science*, **107**, 610–617.

Yang Y., Zhu Z.K., Yin J., Wang X.Y. & Qi Z.E. (1999) Preparation and properties of hybrids of organo-soluble polyimide and montmorillonite with various chemical surface modification methods. *Polymer*, **40**, 4407–4414.

Yu X.F. (2007) The preparation and characterization of cetyltrimethylammonium intercalated muscovite. *Microporous and Mesoporous Materials*, **98**, 70–79.

Yu X.F., Zhao L.Y., Gao X.X, Zhang X.P. & Wu N.Z. (2006) The intercalation of cetyltrimethylammonium cations into muscovite by a two-step process: I. The ion exchange of the interlayer cations in muscovite with Li^+. *Journal of Solid State Chemistry*, **179**, 1569–1574.

Yun Y.H., Han S.P., Lee S.H. & Choi S.C. (2002) Surface modification of sericite using TiO_2 powders prepared by alkoxide hydrolysis: whiteness and SPF indices of TiO_2-adsorbed sericite. *Journal of Materials Synthesis & Processing*, **10**, 359–365.

Zawrah M.F., Khattab R.M., Saad E.M., Gado R.A. (2014) Effect of surfactant types and their concentration on the structural characteristics of nanoclay. *Spectrochimica Acta Part A: Molecular and Biomolecular Spectroscopy*, **122**, 616–623.

Zhang Q., Li D.X., Lai D.W. & Ou B.L. (2015) Hexadecyltrimethylammonium bromide-modified sericite mica-based polyimide composites: a comparison between *in situ* polymerization and solution intercalation Processes. *Macromolecular Research*, **23**, 802–808.

Zhang Q., Li D.X., Lai D.W., You Y.L. & Ou B.L. (2016) Preparation, microstructure, mechanical, and thermal properties of *in situ* polymerized polyimide/organically modified sericite mica composites. *Polymer Composites*, **37**, 2243–2251.

Zhang Y.H., Fu S.Y., Li R.K.Y., Wu J.T., Li L.F., Ji J.H. & Yang S.Y. (2005) Investigation of polyimide–mica hybrid films for cryogenic applications. *Composites Science and Technology*, **65**, 1743–1748.

Zhao W., Xu Y., Song C.R., Chen J. & Liu X.H. (2019) Polyimide/mica hybrid films with low coefficient of thermal expansion and low dielectric constant. *e-Polymers*, **19**, 181–189.

https://doi.org/10.1180/clm.2021.22 Published online by Cambridge University Press